Electronic Supplementary Information

Main chain engineering of phenothiazine-based semiconducting copolymers for stable perovskite solar cells at 85 ºC

Bing Zhang,‡ Yuyan Zhang,‡ Yuefang Wei, Tianyu Li, Jing Zhang, Yi Yuan* and Peng Wang*

E-mail: yyuan@zju.edu.cn; pw2015@zju.edu.cn

1. Experimental section

1.1. Materials

1,4-Dibromo-2,5-dimethoxybenzene (98%, Aladdin), 2-(2,3-dihydrothieno[3,4-b][1,4]dioxin-5-yl)-4,4,5,5-tetramethyl-1,3,2-dioxaborolane (98%, Aladdin), palladium diacetate (Pd(OAc)$_2$, 99%, Energy Chemical), 2-dicyclohexylphosphino-2',6'-dimethoxybiphenyl (SPhos, 98%, Energy Chemical), potassium phosphate (K$_3$PO$_4$, 98%, Energy Chemical), 1,4-dioxane (99%, Energy Chemical), 3,4-ethylenedioxythiophene (EDOT, 98%, Bidepharm), tris(o-tolyl)phosphine (P(o-tolyl)$_3$, 98%, Energy Chemical), pivalic acid (PivOH, 99%, Energy Chemical), potassium carbonate (K$_2$CO$_3$, 99%, Energy Chemical), N,N-dimethyl acetamide (DMAc, 99.8%, Energy Chemical), deuterated THF (THF-d_8, 99.8%, Energy Chemical), deuterated chloroform (CDCl$_3$, 99.8%, Energy Chemical), 1-ethyl-3-methylimidazolium bis(trifluoromethanesulfonyl)imide (EMITFSI, 98%, Energy Chemical), ferrocene (Fc, 99%, Macklin), tetrahydrofuran (THF, 99%, Sinopharm Chemical Reagent Co., Ltd), acetone (99.5%, Energy Chemical), ethanol (99.7%, Aladdin), chlorobenzene (CB, 99.8%, Acros Organics), acetonitrile (99.8%, Aladdin), 4-$tert$-butylpyridine (TBP, 96%, Sigma-Aldrich), benzocyclobutene (BCB, 98%, Energy Chemical), titanium diisopropoxide bis(acetylacetonate) (TIACA, 75% in isopropanol, Sigma-Aldrich), acetylacetone (ACAC, 99.0%, TCI), TiO$_2$ paste (30NR-D, Greatcell Solar), lead iodide (PbI$_2$, 99.99%, TCI), lead bromide (PbBr$_2$, 99.99%, TCI), formamidinium iodide (FAI, 99.0%, Greatcell Solar), methylammonium bromide (MABr, 99.0%, Greatcell Solar), cesium iodide (CsI, 99.0%, TCI), zinc iodide (ZnI$_2$, 99.995%, Alfa Aesar), hexakis(methoxymethyl)melamine (HMMM, 98%, Aladdin), isopropanol (IPA, 99.9%, Energy Chemical), dimethylsulfoxide (DMSO, 99.9%, Sigma-Aldrich), N,N-dimethylformamide (DMF, 99.8%, Sigma-Aldrich), poly(9-vinylcarbazole) (PVK, average M_n = 25,000−50,000, Sigma Aldrich), poly[bis(4-phenyl)(2,4,6-trimethylphenyl)amine] (PTAA, Merck), $N^2,N^2,N^{2'},N^{2'},N^7,N^7,N^{7'},N^{7'}$-octakis(4-methoxyphenyl)-9,9'-spirobi[fluorene]-2,2',7,7'-tetraamine (spiro-OMeTAD, 99.8%, Xi'an Polymer Light Technology Corp.) and other solvents were purchased from commercial sources and used as received without further purification. Deionized water with resistivity greater than 18 MΩ cm was provided by an UPR-II-10T Ultrapure water system (ULUPURE). 3,7-Dibromo-10-(2-octyldodecyl)phenothiazine and 4-$tert$-butylpyridinium bis(trifluoromethanesulfonyl)imide (TBPHTFSI) were synthesized according to the literature methods.[1,2]

1.2. General instrumentation

The ^{1}H nuclear magnetic resonance (NMR) and ^{13}C NMR spectra were recorded using AVANCE III 400 and III 500 NMR spectrometers (Bruker). High-resolution mass spectra (HR-MS) were acquired with an Ultraflex

Xtreme MALDI-TOF mass spectrometer (Bruker). Attenuated total reflection-Fourier transform infrared (ATR-FTIR) spectra were collected using a Vector 22 FTIR spectrometer (Bruker). Ultraviolet-visible (UV-Vis) absorption spectra were measured using a Cary 8454 spectrophotometer (Agilent Technologies). High-temperature gel permeation chromatography (HT-GPC) measurements were performed using the PL-GPC220 instrument (Polymer Laboratories Ltd.) with 1,2,4-trichlorobenzene as the solvent. Cyclic voltammetric (CV) measurements were conducted on a CHI660E electrochemical workstation (CH Instruments) equipped with a three-electrode electrolytic cell: a glassy carbon working electrode, a fluorine-doped tin oxide (FTO) counter electrode, and an Ag/AgCl (sat. KCl) reference electrode. The electrolyte employed in this study consisted of a 0.1 M EMITFSI solution in acetonitrile. Time-resolved PL (TRPL) decays were obtained using a Life-Spec-II fluorescence spectrometer (Edinburgh Instruments Ltd). The thicknesses of the thin films were measured using a D-500 stylus profilometer (KLA-Tencor). Ultraviolet photoelectron spectra (UPS) were measured using an ESCALAB XI+ instrument (Thermo Fisher). Differential scanning calorimetry (DSC) measurements were carried out using a DSC Q100 V9.7 Build 291 instrument (TA) at a heating rate of 10 $^{\circ}$C min^{-1} under a flowing nitrogen atmosphere. Water contact angles of the thin films were measured using a DropMeter™ A-100P contact angle meter (Maist Co. Ltd.). Transmission polarization optical microscope (POM) images were recorded using an SDPTOP CX40P system (Sunny Optical Technology). Top-viewed surface morphologies were observed with a SU-70 field emission scanning electron microscope (SEM, Hitachi). Fluorescence optical microscope (FOM) images were obtained using an ECLIPSE Ti-U system (Nikon). X-ray diffraction (XRD) patterns were collected using a SmartLab diffractometer (Rigaku) operating at 7200 W power (40 kV, 180 mA) with Cu Kα radiation (λ=0.15418 nm).

1.3. Synthesis

1.3.1. 5-[4-(2,3-Dihydrothieno[3,4-*b*][1,4]dioxin-5-yl)-2,5-dimethoxyphenyl]-2,3-dihydrothieno[3,4-*b*][1,4]dioxine (EBEM)

In a round bottom flask, 1,4-dibromo-2,5-dimethoxybenzene (1.5 g, 5.0 mmol), 2-(2,3-dihydrothieno[3,4-*b*][1,4]dioxin-5-yl)-4,4,5,5-tetramethyl-1,3,2-dioxaborolane (3.4 g, 12.5 mmol), Pd(OAc)$_2$ (56.1 mg, 0.25 mmol), SPhos (102.6 mg, 0.25 mmol), K$_3$PO$_4$ (3.2 g, 15.0 mmol), water (10 mL), and 1,4-dioxane (50 mL) were combined. The flask was subjected to evacuation and purged with argon three times. The resulting reaction mixture was stirred at 60 $^{\circ}$C for 24 h. After cooling to room temperature, water (40 mL) was added, followed by three extractions with dichloromethane. The organic phase was combined and concentrated under reduced

3

pressure. The crude product was purified by column chromatography on silica gel (THF/petroleum ether, v/v, 1/5; 60–90 °C) to yield the desired white powder (1.8 g, 86% yield). ^{1}H NMR (500 MHz, CDCl$_3$) δ: 7.69 (s, 2H), 6.39 (s, 2H), 4.31 (d, J = 4.0 Hz, 2H), 4.26 (d, J = 4.0 Hz, 2H), and 3.90 (s, 6H) ppm. ^{13}C NMR (125 MHz, CDCl$_3$) δ 149.90, 141.35, 138.80, 121.04, 113.27, 113.14, 99.68, 64.99, 64.46, and 56.72 ppm. HR-MS (MALDI-TOF) m/z calcd. for [M+H]$^+$: 418.0540. Found: 418.0539. ATR-FTIR (film) v_{max}: 2955, 2923, 2853, 2717, 2048, 1732, 1574, 1517, 1462, 1440, 1398, 1363, 1279, 1219, 1165, 1067, 1044, 1027, 932, 901, 869, 827, 750, and 711 cm^{-1}.

1.3.2. p-PTZ-E

A Schlenk reaction tube was charged with 3,7-dibromo-10-(2-octyldodecyl)phenothiazine (500.0 mg, 0.78 mmol), EDOT (111.6 mg, 0.78 mmol), Pd(OAc)$_2$ (18.0 mg, 0.08 mmol), P(o-tolyl)$_3$ (47.7 mg, 0.16 mmol), PivOH (40.8 mg, 0.40 mmol), K$_2$CO$_3$ (325.7 mg, 2.36 mmol), and N,N-dimethylacetamide (100 mL). The reaction vessel was then evacuated and purged with argon three times. The resulting reaction mixture was stirred at 150 °C for 3 h. Upon cooling to room temperature, the solvent was removed under reduced pressure. The crude product was purified by column chromatography on silica gel using a sequential elution with toluene/petroleum ether (v/v, 1/1; 60–90 °C) followed by toluene/THF (v/v, 1/1). The fraction eluted with toluene/THF was concentrated to 20 mL and added dropwise to vigorously stirred methanol (200 mL). The resulting suspension was filtered through a Millipore hydrophobic PTFE membrane (pore size: 0.22 μm). The obtained residue was dried under vacuum at 60 °C, yielding a yellow powder (72%, 348.8 mg). ^{1}H NMR (400 MHz, THF-d_8) δ: 7.58 (s, 2H), 7.50 (d, J = 7.6 Hz, 2H), 6.93 (d, J = 8.0 Hz, 2H), 4.34 (s, 4H), 3.80 (s, 2H), 2.02 (s, 1H), 1.32–1.20 (m, 32H), and 0.87 (t, J = 6.6 Hz, 6H) ppm. ^{13}C NMR (100 MHz, THF-d_8) δ: 144.88, 139.57, 128.94, 126.51, 125.55, 125.43, 116.95, 114.41, 65.77, 52.30, 35.96, 33.07, 33.05, 32.66, 31.17, 30.79, 30.62, 30.59, 30.51, 27.38, 27.37, 25.49, 23.76, and 14.68 ppm. ATR-FTIR (film) v_{max}: 2955, 2923, 2853, 1737, 1655, 1464, 1360, 1262, 1158, 1090, 1021, 856, 811, and 752 cm^{-1}.

1.3.3. p-PTZ-EBEM

A Schlenk reaction tube was charged with 3,7-dibromo-10-(2-octyldodecyl)phenothiazine (500.0 mg, 0.78 mmol), EBEM (326.4 mg, 0.78 mmol), Pd(OAc)$_2$ (18.0 mg, 0.08 mmol), P(o-tolyl)$_3$ (47.7 mg, 0.16 mmol), PivOH (40.8 mg, 0.40 mmol), K$_2$CO$_3$ (325.7 mg, 2.36 mmol), and N,N-dimethylacetamide (100 mL). The reaction vessel was then evacuated and purged with argon three times. The resulting reaction mixture was stirred at 150 °C for 3 h. After cooling to room temperature, the solvent was removed under reduced pressure. The crude

4

product was purified by column chromatography on silica gel, sequentially eluting with toluene/petroleum ether (v/v, 1/1; 60–90 ºC) followed by toluene/THF (v/v, 1/1). The fraction eluted with toluene/THF was condensed to 20 mL and added dropwise to vigorously stirred methanol (200 mL). The resulting suspension was filtered through a Millipore hydrophobic PTFE membrane (pore size: 0.22 μm). The obtained residue was dried under vacuum at 60 ºC, affording an orange powder (89%, 623.9 mg). ^{1}H NMR (400 MHz, THF-d_8) δ: 8.32 (s, 1H), 8.05−7.85 (m, 3H), 7.68−7.45 (m, 3H), 6.94 (d, J = 7.2 Hz, 1H), 4.40 (d, J = 16.7 Hz, 8H), 4.01−3.81 (m, 8H), 2.04 (s, 1H), 1.35−1.16 (m, 32H), and 0.87 (t, J = 4.5 Hz, 6H) ppm. ^{13}C NMR (100 MHz, THF-d_8) δ: 150.71, 150.67, 144.84, 142.57, 140.62, 140.57, 140.03, 138.58, 138.55, 129.35, 126.47, 125.74, 125.56, 122.05, 121.82, 121.81, 116.86, 116.58, 116.51, 114.10, 113.36, 113.32, 111.72, 111.67, 100.29, 66.04, 65.86, 65.54, 65.31 56.87, 56.75, 52.28, 36.02, 33.07, 33.06, 32.71, 31.20, 30.80, 30.63, 30.60, 30.51, 30.47, 27.42, 25.49, 23.76, and 14.68 ppm. ATR-FTIR (film) v_{max}: 2956, 2923, 2853, 1738, 1463, 1398, 1363, 1220, 1161, 1087, 932, 856, 818, and 746 cm^{-1}.

1.4. Direct-current electrical conductivity

A hole transport layer was deposited onto interdigital gold electrodes through spin-coating a chlorobenzene solution at 1000 rpm. The solution was prepared by dissolving 40 mg mL^{-1} of a semiconducting polymer, along with 132 mM of TBP and TBPHTFSI at concentrations of 0, 2.1, 3.2, 4.4, or 7.1 mg mL^{-1}. The interdigital gold electrode consisted of 119 channels, each having a length (L) of 1.5 mm, a width (W) of 10 μm, and a thickness (t) of 110 nm. Prior to the current–voltage ($I–V$) measurement using a Keithley 2400 source meter, the sample was stored in a dry air environment (<5% RH) for one week. The $I–V$ curve was obtained within the voltage range of –1.0 V to 1.0 V. The direct-current electrical conductivity (σ) was determined by using the equation $\sigma = s\dfrac{W}{119Lt}$, where s refers to the slope derived from the linear fitting of the $I–V$ curve.

1.5. Hole density

To quantify the hole density (p) of the exclusively semiconducting polymer-based hole transport layer, a metal-insulator-semiconductor (MIS) device was employed. The MIS device followed an architecture of n^{++}-Si/SiO$_2$/p-BCB/HTL/Au, where p-BCB denoted polybenzocyclobutene. The p-BCB layer was grown on heavily n-type doped Si with a 300 nm SiO$_2$ coating, which was achieved through annealing a BCB layer at 250 ºC for 1 h. Deposition of the BCB layer was accomplished by spin-coating a 1 mg mL^{-1} BCB solution in CB. Subsequently, the semiconducting polymer layer was spin-coated onto the p-BCB layer, followed by vacuum deposition of the

gold layer. The Autolab PGSTAT302N electrochemical workstation was employed to record the impedance

spectra of the MIS device under various bias potentials (V). The capacitance (C) was calculated using the

equation $C = -\dfrac{1}{\omega}\left[\dfrac{Z'' - \omega L_i}{\left(Z' - R_s\right)^2 + \left(Z'' - \omega L_i\right)^2}\right]$, with Z' and Z'' representing the real and imaginary parts of the

impedance spectra, respectively. R_s denoted the series resistance, L_i represented the parasitic inductance, and w

was the angular frequency. The $C - V$ curves exhibited distinct accumulation and depletion regimes for the

semiconducting polymer layer. To determine the p value, the equation $p = \dfrac{2}{q\varepsilon_r\varepsilon_0 \dfrac{d\left(A/C\right)^2}{dV}}$ was employed,

where q denoted the elementary charge, ε_r referred to the relative permittivity, ε_0 represented the vacuum

permittivity, and A indicated the area of the MIS device. However, assessing the p value of semiconducting

polymer composite layers containing TBPHTFSI proved irreproducible using the MIS device, probably due to

the ion drift. To overcome this limitation, a comparison approach based on the quadratic integral intensity of the

electron paramagnetic resonance (EPR) signal was adopted. By comparing the EPR signals of the

semiconducting polymer layer with and without TBPHTFSI and considering the known p value of the layer

without TBPHTFSI, the p value of the semiconducting polymer composite layer containing TBPHTFSI was

estimated. Specifically, a 2 cm × 2 cm × 0.5 mm cover glass was used as a substrate to spin-coat a

semiconducting polymer layer with or without TBPHTFSI, which was subsequently stored in dry air for one

week. The resulting sample was crushed and loaded into a borosilicate glass tube for EPR measurement using an

A300-10/12 spectrometer (Bruker).

1.6. Fabrication of perovskite solar cell

The laser-etched fluorine-doped tin oxide (FTO) glass (TEC 14, Nippon Sheet Glass Co., Ltd, white glass, 1.6

mm thickness, 25 mm × 16 mm) underwent a series of ultrasonic cleanings with detergent, deionized water,

acetone, and ethanol. Subsequently, a compact TiO_2 (c-TiO_2) layer was deposited onto the FTO glass at 450 °C

via spray pyrolysis of an alcoholic solution of TIACA (40 mM) and ACAC (400 mM). Next, a mesoporous TiO_2

layer with a thickness of approximately 200 nm was spin-coated from a TiO_2 colloidal solution formulated with

commercial 30NR-D TiO_2 paste at 4000 rpm for 10 s. The resulting film was solidified at 80 °C in air for 10 min

and further sintered at 450 °C with a flow of dry air for 30 min to remove all carbon components. Prior to use, the

cleaned FTO substrate was treated with ultraviolet ozone. The perovskite precursor solution was prepared by

dissolving 1.30 M of PbI_2, 1.19 M of FAI, 0.14 M of $PbBr_2$, 0.14 M of MABr, and 0.07 M of CsI into a mixture

of DMSO and DMF (v/v, 1/4). The deposition of the triple cation perovskite film[3] involved a two-step spin-coating process at 1000 rpm for 10 s (ramp rate 200 rpm s^{-1}) and 6000 rpm for 30 s (ramp rate 2000 rpm s^{-1}). Notably, at 15 s before the spin end, 150 μL CB was dripped onto the substrate. The deposited film was annealed at 120 °C for 1 h to achieve a black perovskite film. Subsequently, a 50 μL IPA solution of ZnI_2 (4 mg mL^{-1}) was dropped on top of the perovskite film and spun at 3000 rpm for 30 s. The film was then annealed at 80 °C in the dark for 10 min to form an ultrathin PbI_2 interlayer.[4] Next, an isopropanol solution of hexakis(methoxymethyl)melamine (2 mg mL^{-1}) was spin-coated onto the perovskite layer, resulting in an ultrathin interlayer of melamine-formaldehyde resin after heating at 80 °C for 30 min.[5] Following this, a hole transport layer was deposited using a chlorobenzene solution containing 20 mg mL^{-1} of a semiconducting polymer, 1.6 mg mL^{-1} of TBPHTFSI, and 132 mM of TBP at 5000 rpm. Finally, an 80 nm thick gold electrode was deposited to complete the device fabrication through thermal evaporation under a vacuum of less than 10^{-4} Pa. The device was stored in dry air (< 5% RH) overnight, covered with waterproof adhesive tape (3M), and further sealed with an epoxy adhesive (3M). The active area of our cells was approximately 0.5×0.5 cm^2. For specific characterizations, the encapsulation materials, gold electrode, and HTL were removed as required.

1.7. Photocurrent-voltage curve and external quantum efficiency spectrum

The AM1.5G sunlight, with an irradiation of 100 mW cm^{-2}, was provided by an LS1000-4S-AM solar simulator (Solar Light Company, USA). The photocurrent density−voltage ($J-V$) curves were measured using a Keithley 2400 source meter in conjunction with Labview 14.0. The photoactive area of the perovskite solar cells was defined by a metal mask with an aperture area of 0.16 cm^2. External quantum efficiency (EQE) spectra were measured using an Omni-λ300 monochromator (Zolix, China) equipped with a 150 W xenon lamp (Zolix, China). Photocurrent was recorded using a computer-controlled Keithley 2400 source meter. The monochromatic light intensity was measured using a Hamamatsu S1337-1010BQ silicon diode, which was calibrated at the National Institute of Metrology, China.

1.8. Operation stability and thermostability tests

Maximal power point (MPP) tracking of perovskite solar cells was conducted within a nitrogen-filled glovebox using a 16-channel photovoltaic tracking system (YH Electronic Equipment Business) and an SLS-LED80A solar simulator (Qingdao Solar Scientific Instrument High-tech Co., LTD). MPP data were collected at two-minute intervals employing the standard perturb and observe method. To assess the thermostability of perovskite

solar cells, $J-V$ measurements under AM1.5G conditions were periodically performed while subjecting the cells to an FD56 oven (Binder, Germany) at temperatures of 85 ^{o}C. The atmospheric humidity outside the oven ranged between 40% and 90%.

2. Theoretical modelling

2.1. Molecular geometry, frontier molecular orbital, and energy level

The molecular geometry, frontier molecular orbitals, and energy levels were calculated using the Gaussian 16 program suite within the framework of periodic boundary condition-density functional theory (PBC-DFT) at the B3LYP/6-311G(d,p) level of theory.

2.2. Glass transition

We utilized the Build Polymer tool available in Material Studio 8.0 to construct p-PTZ-E and p-PTZ-EBEM polymers with a degree of polymerization of 10. Subsequently, the Amorphous Cell module was employed to generate a cubic box with periodic boundaries, containing either 10 polymer chains or 10 polymer chains combined with TBPHTFSI molecules at a weight percentage of 7.5%. To investigate the properties of these systems, molecular dynamics (MD) simulations were conducted using the COMPASS II force field. Moreover, we utilized the FORCITE module in Materials Studio 8.0 to explore the glass transition temperature (T_g). Our simulation protocol involved an initial NVT simulation at 800 K using a Nose thermostat, followed by an NPT simulation at the same temperature employing both a Nose thermostat and a Berendsen barostat. Subsequently, a stepwise cooling process was performed from 800 K to 200 K, with NVT and NPT simulations conducted at each temperature. The equilibrated specific volumes (SV) were recorded at each temperature. By determining the intersection of the linear fitting lines in the low and high temperature regions, we obtained the theoretical T_g, denoted as T_g^{SV}.

3. References

1 H. Saito, J. Chen, J. Kuwabara, T. Yasuda and T. Kanbara, *Polym. Chem.*, 2017, **8**, 3006.

2 Y. Ren, M. Ren, X. Xie, J. Wang, Y. Cai, Y. Yuan, J. Zhang and P. Wang, *Nano Energy*, 2021, **81**, 105655.

3 M. Saliba, T. Matsui, J.-Y. Seo, K. Domanski, J.-P. Correa-Baena, M. K. Nazeeruddin, S. M. Zakeeruddin, W. Tress, A. Abate, A. Hagfeldt and M. Grätzel, *Energy Environ. Sci.*, 2016, **9**, 1989.

4 T. Li, M. Ren, Y. Zhang, L. Fang, J. Zhang, Y. Yuan, J. Zhang and P. Wang, *Small*, 2020, **16**, 2001866.

5 T. Li, Y. Zhang, L. Fang, B. Zhang, Y. Yuan, J. Zhang and P. Wang, *J. Mater. Chem. A*, 2023, **11**, 10.1039/D3TA03314G.

4. Additional data

Table S1 Fitting parameters of time-resolved PL decays, time constants, and yields of hole extraction [a]

Sample	τ_1 [ns]	A_1	τ_2 [ns]	A_2	τ [ns]	τ_p [ns]	ϕ_p [%]
CsMAFA	469.5	0.13	2324.0	0.87	2082.9	/	/
CsMAFA/p-PTZ-E	4.2	0.16	41.4	0.84	35.4	36.0	98.3
CsMAFA/p-PTZ-EBEM	1.7	0.29	23.7	0.71	17.4	17.5	99.2

[a] Time-resolved PL decays were fitted by biexponential functions. The parameters τ_1 and τ_2 are the time constants of fast and slow decays, respectively, whereas A_1 and A_2 represent the relative amplitudes of these decays. τ is the amplitude-averaged time constant which is calculated by equation $\tau = A_1\tau_1 + A_2\tau_2$. The time constant of hole extraction (τ_p) can be calculated by equation $\tau_p = \dfrac{\tau_w \tau_{w/o}}{\tau_{w/o} - \tau_w}$, where $\tau_{w/o}$ and τ_w are the amplitude-averaged PL lifetimes of CsMAFA covered without and with a semiconducting polymer, respectively. The yield of hole extraction (ϕ_p) can be determined by equation $\phi_p = \dfrac{\tau_{w/o} - \tau_w}{\tau_{w/o}}$.
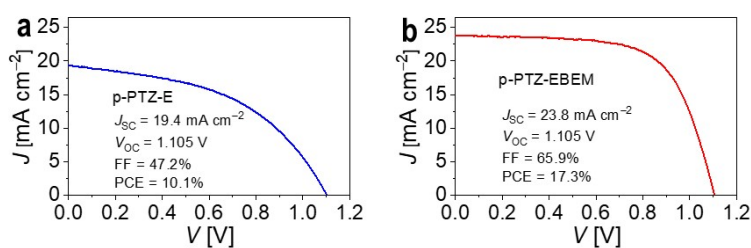
Fig. S1 *J–V* curves measured under the AM1.5G conditions for PSCs with (a) p-PTZ-E and (b) p-PTZ-EBEM.
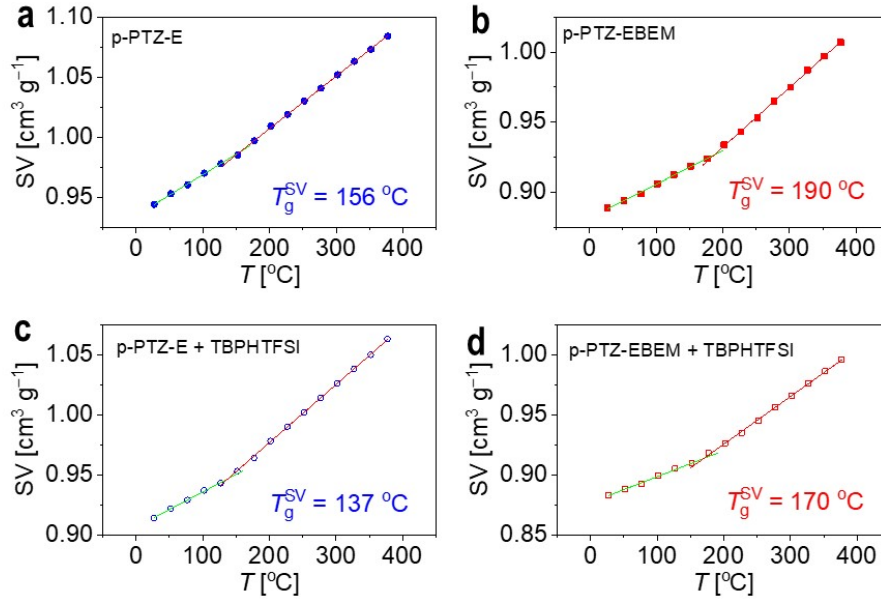
Fig. S2 Plots of the specific volume (SV) as a function of temperature (T), obtained from molecular dynamics simulation. The green and redx lines depict the linear fits of the low-temperature and high-temperature regions, respectively. The theoretical glass transition temperature (T_g^{SV}) can be determined by the intersection of the linear fits.
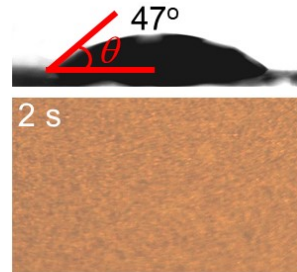
Fig. S3 Water contact angle (θ) and polarized optical microscopy (POM) image 2s after dripping a water droplet CsMAFA perovskite on glass.
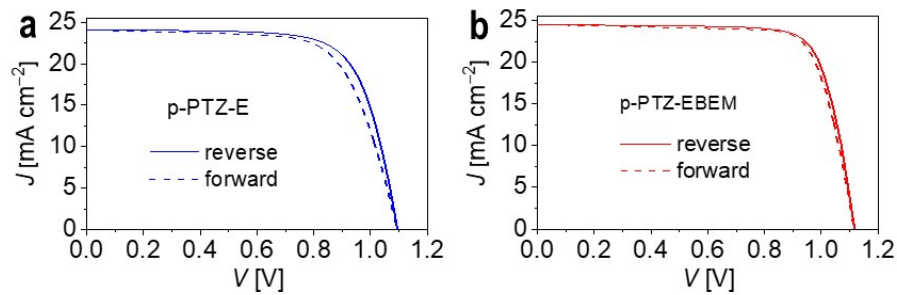
Fig. S4 Forward and reverse scans of p-PTZ-E cell and p-PTZ-EBEM cell.
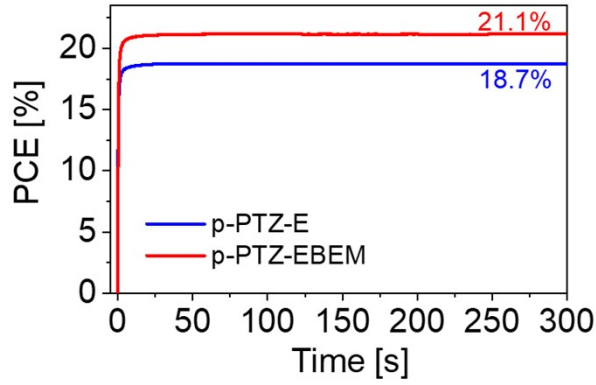
Fig. S5 Maximum power point (MPP) tracking of a representative PSC with either p-PTZ-E or p-PTZ-EBEM as HTL.
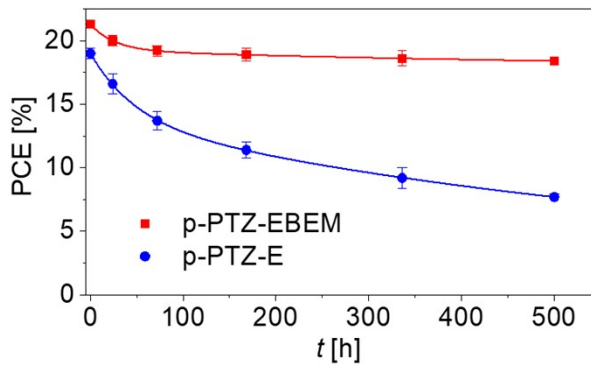
Fig. S6 Temporal evolutions of the efficiency of solar cells aged at 85 °C.
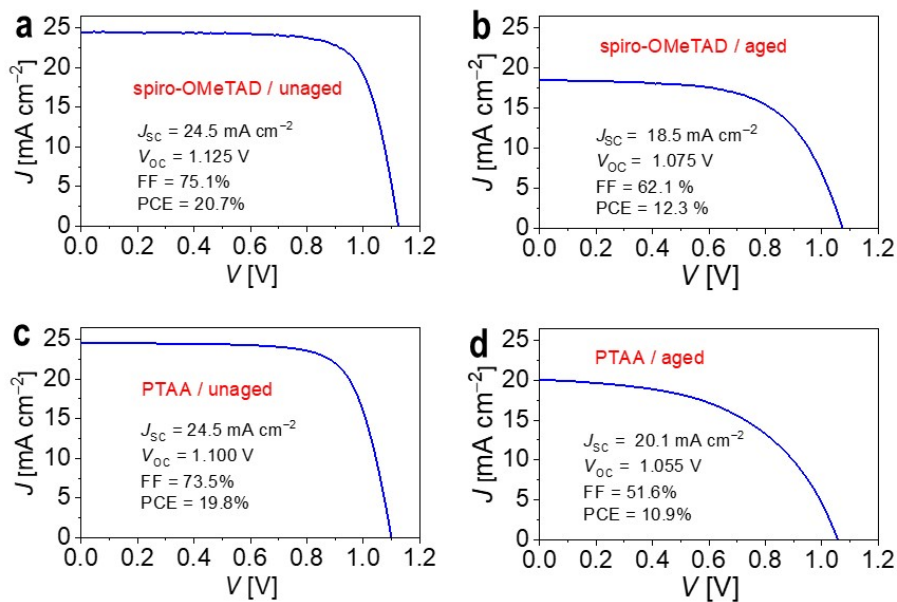
Fig. S7 $J–V$ curves measured under the AM1.5G conditions for the unaged and aged PSCs with (a,b) spiro-OMeTAD and (c,d) PTAA. The aging was performed in an oven at 85 °C for 500 h.
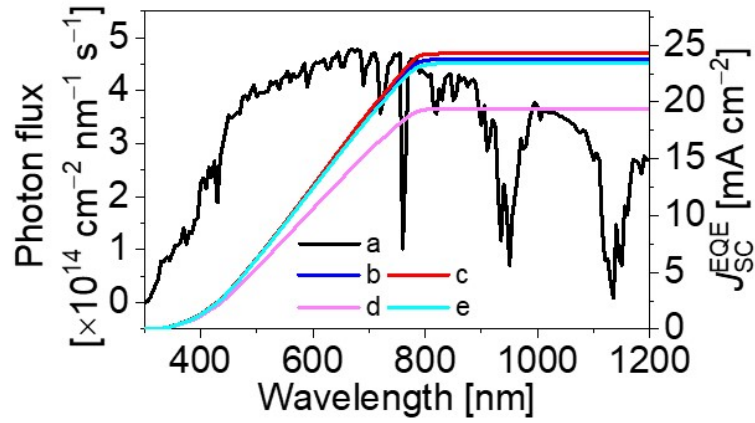
Fig. S8 The ASTM G173 AM1.5G spectral photon flux (a). The photocurrent densities predicted from the EQE spectra (J_{SC}^{EQE}) of the unaged cell with p-PTZ-E (b), the unaged cell with p-PTZ-EBEM (c), the aged cell with p-PTZ-E (d), and the aged cell with p-PTZ-EBEM (e). The aging was performed at 85 °C for 500 h.
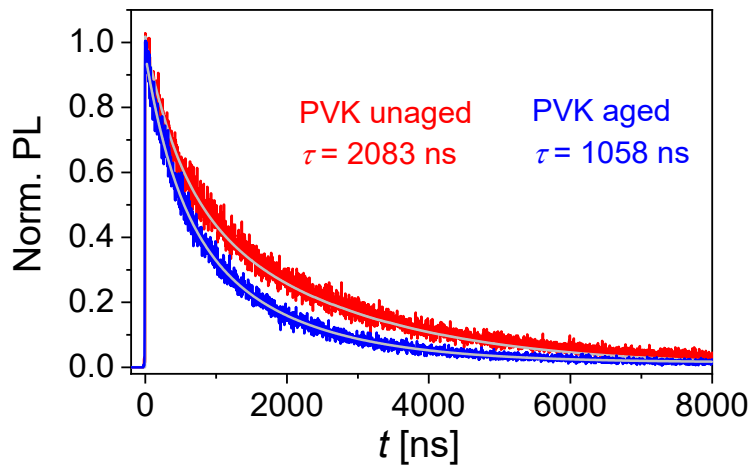
Fig. S9 Time-resolved PL traces at 785 nm of encapsulated dummy cells (glass/CsMAFA/PVK/gold) before and after 500 h aging at 85 °C. PVK refers to poly(9-vinylcarbazole).

5. Appendix: ^{1}H NMR spectra, ^{13}C NMR spectra, HR-MS, and ATR-FTIR spectra
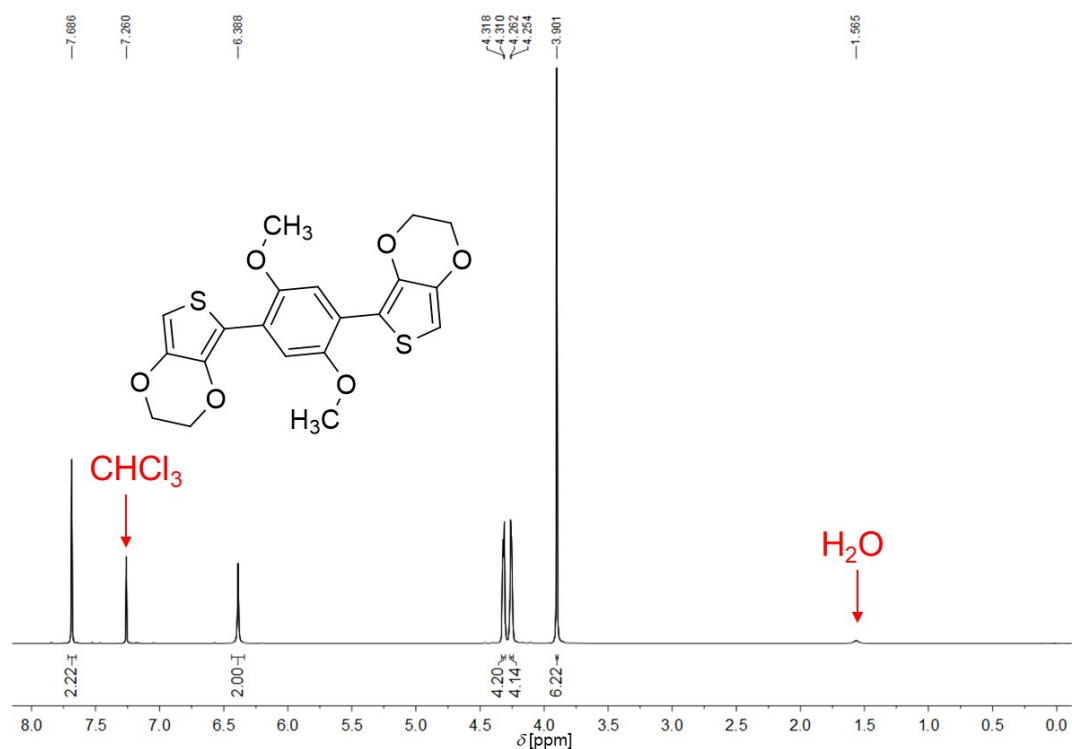
Fig. S10 ^{1}H NMR (500 MHz) spectrum of EBEM in CDCl$_3$.
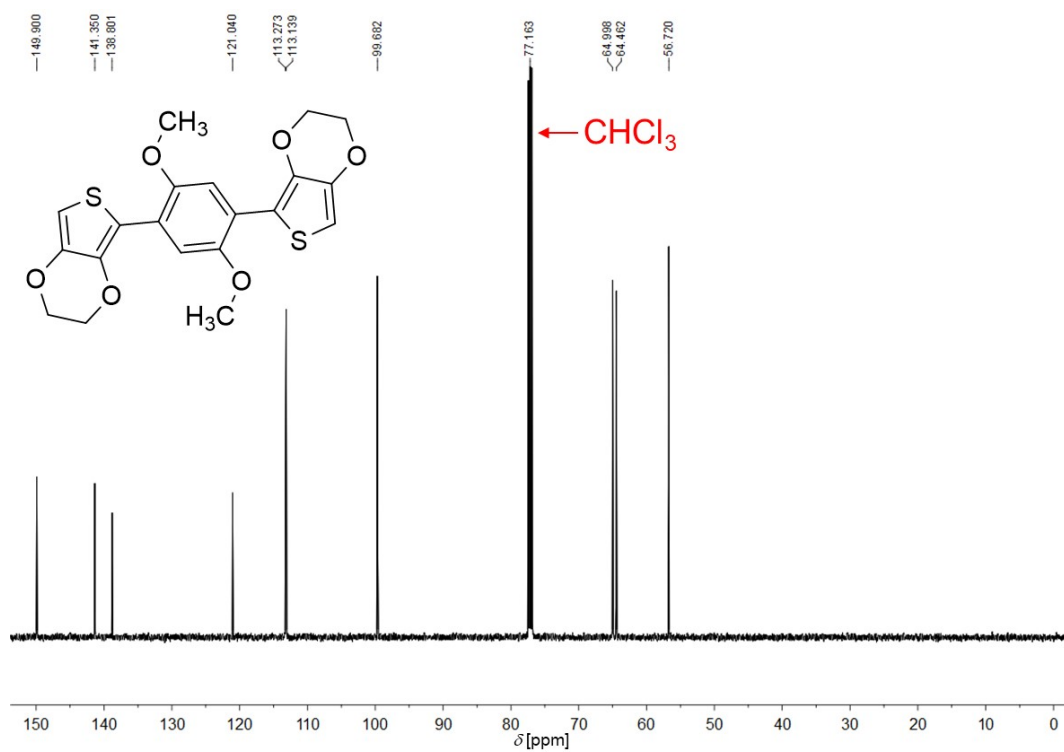
Fig S11 ^{13}C NMR (125 MHz) spectrum of EBEM in CDCl$_3$.
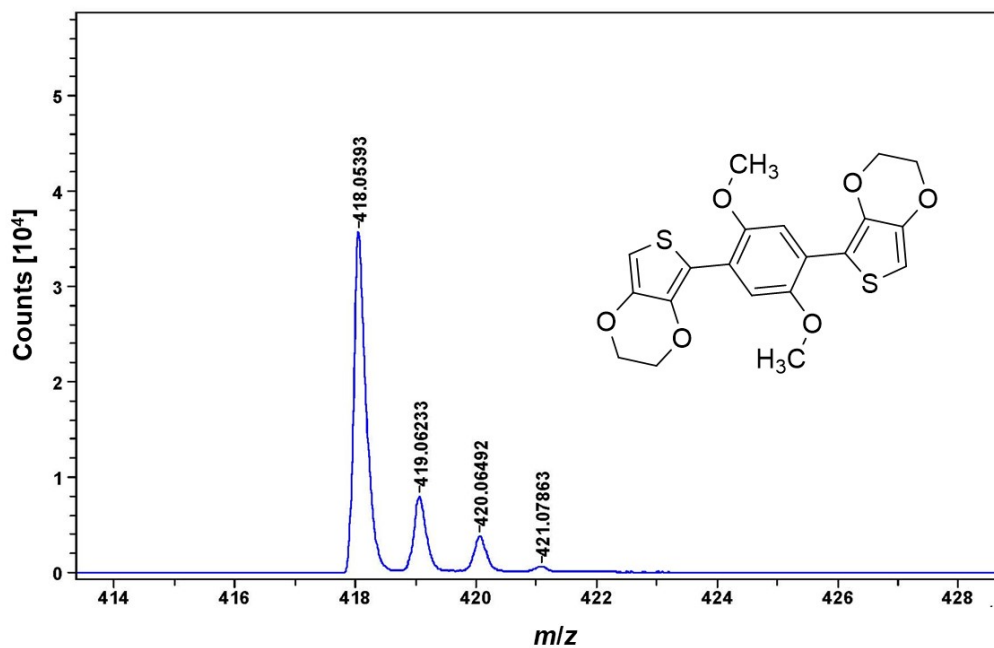
Fig. S12 HR-MS of EBEM.
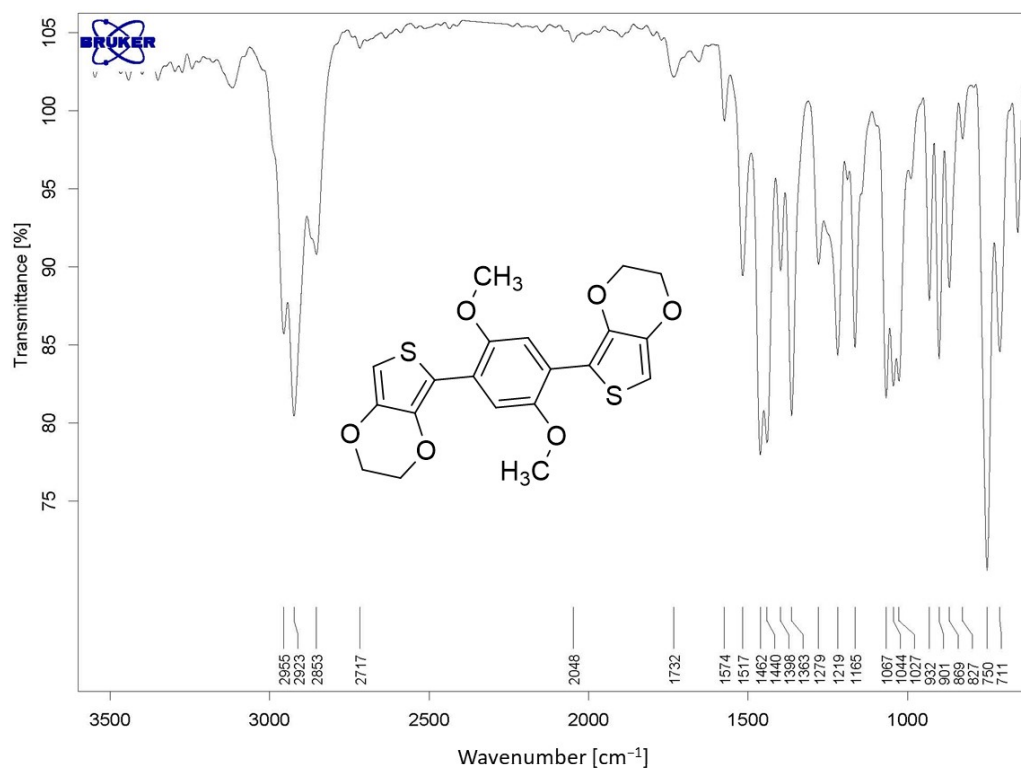
Fig. S13 ATR-FTIR spectrum of EBEM.

14
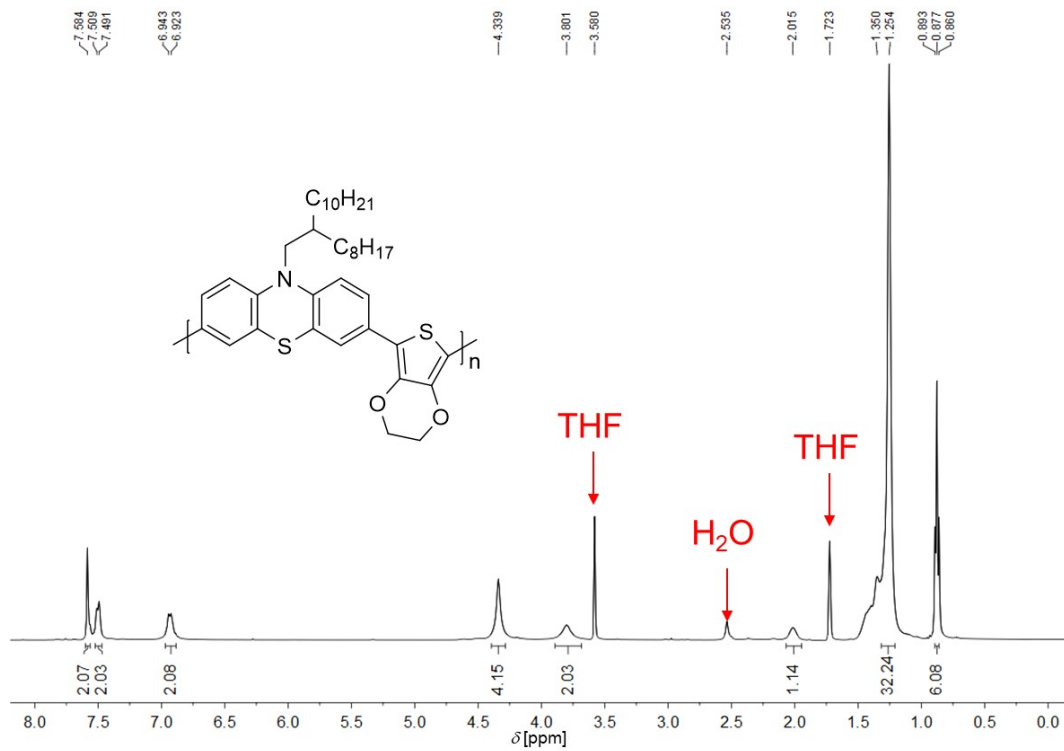
Fig. S14 ¹H NMR (400 MHz) spectrum of p-PTZ-E in THF-d_8.
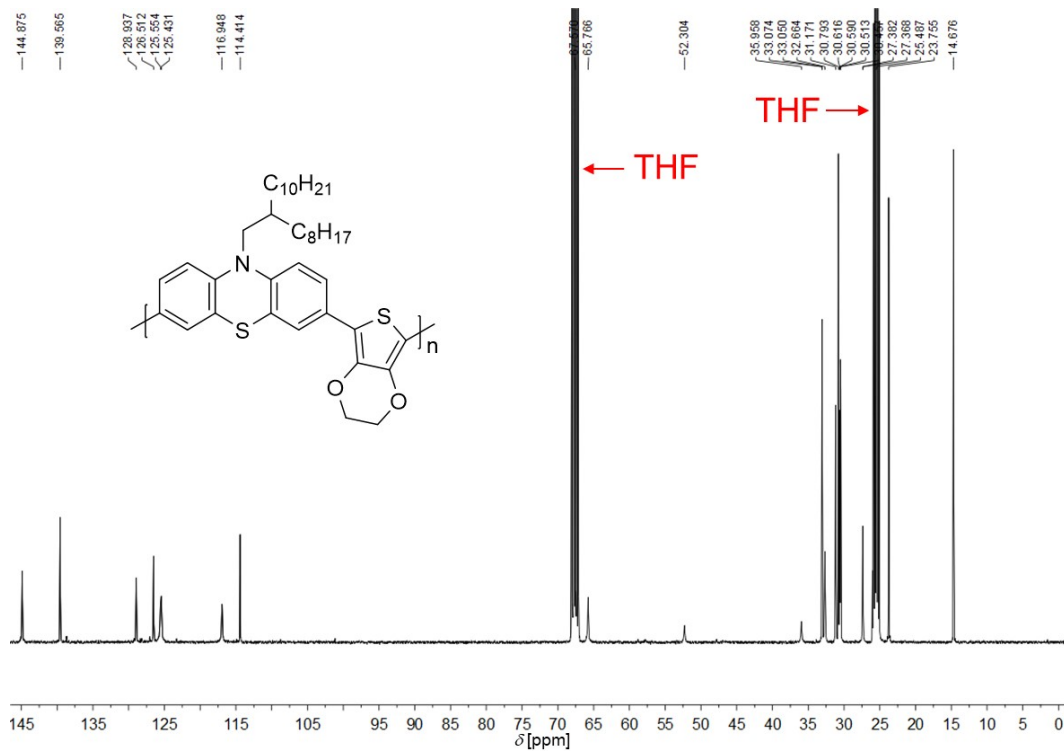
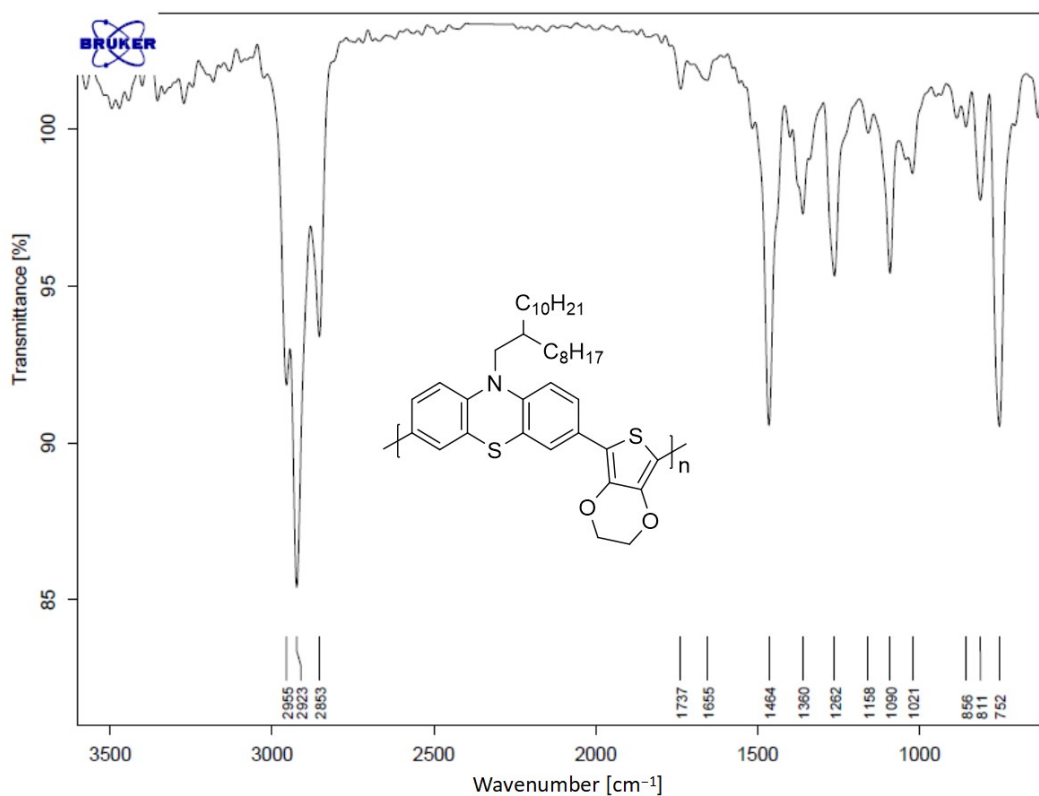**Fig. S15** ¹³C NMR (100 MHz) spectrum of p-PTZ-E in THF-d_8.

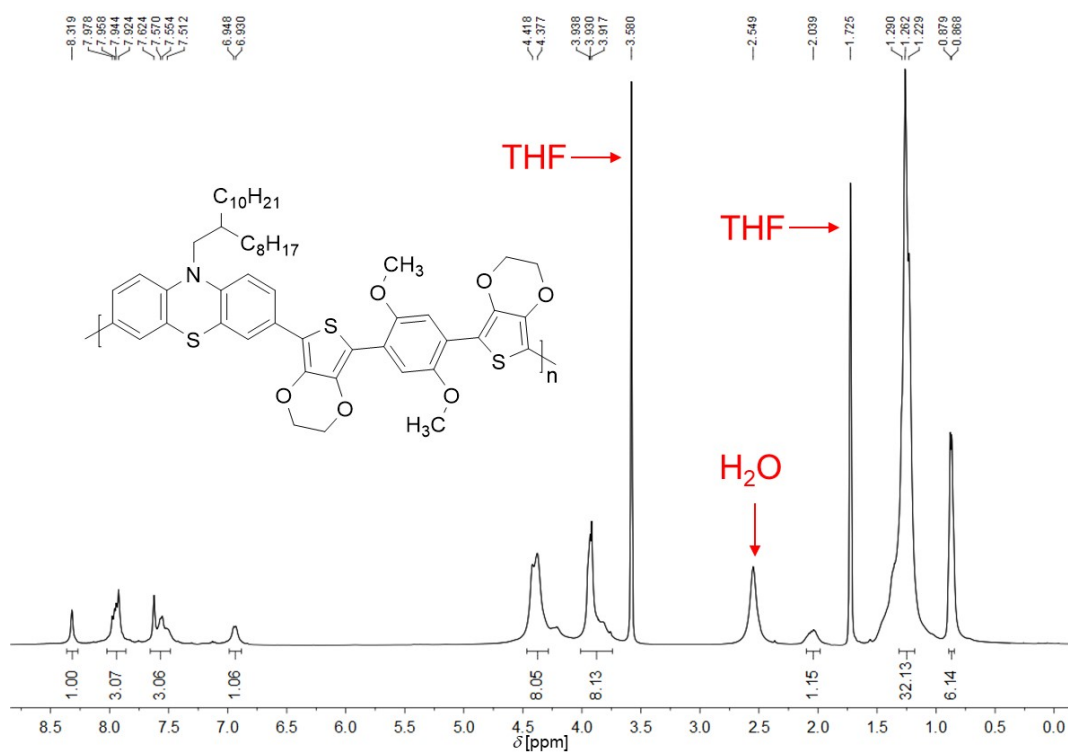**Fig. S16** ATR-FTIR spectrum of p-PTZ-E.

Fig. S17 ^{1}H NMR (400 MHz) spectrum of p-PTZ-EBEM in THF-d_8.
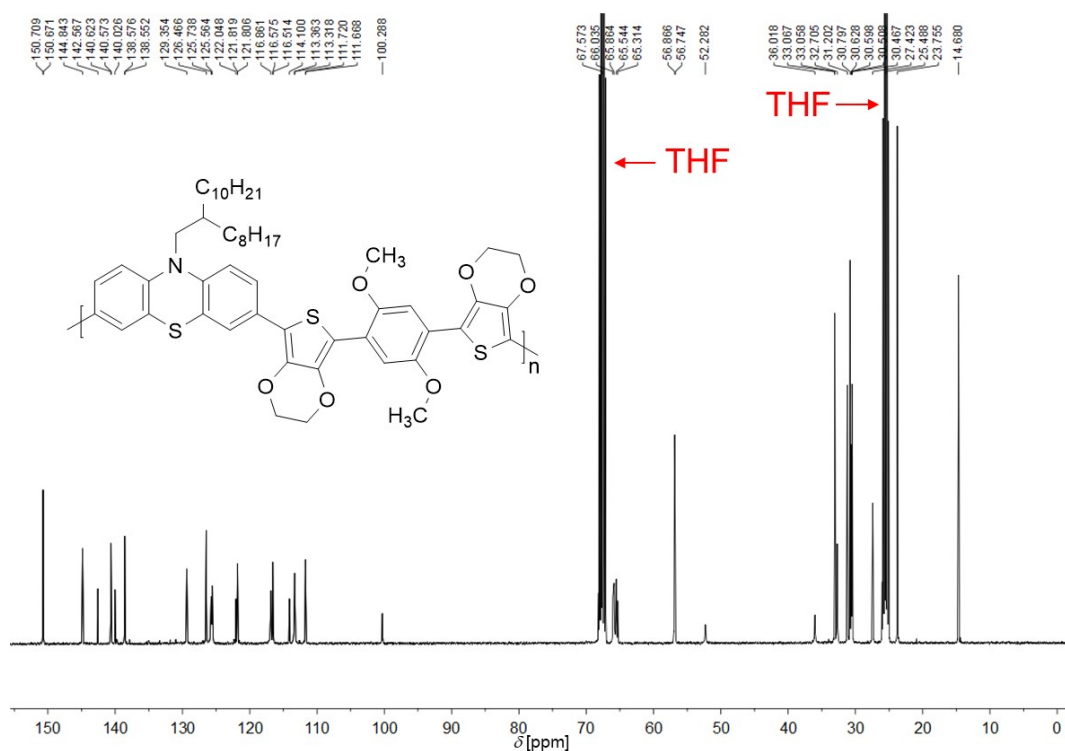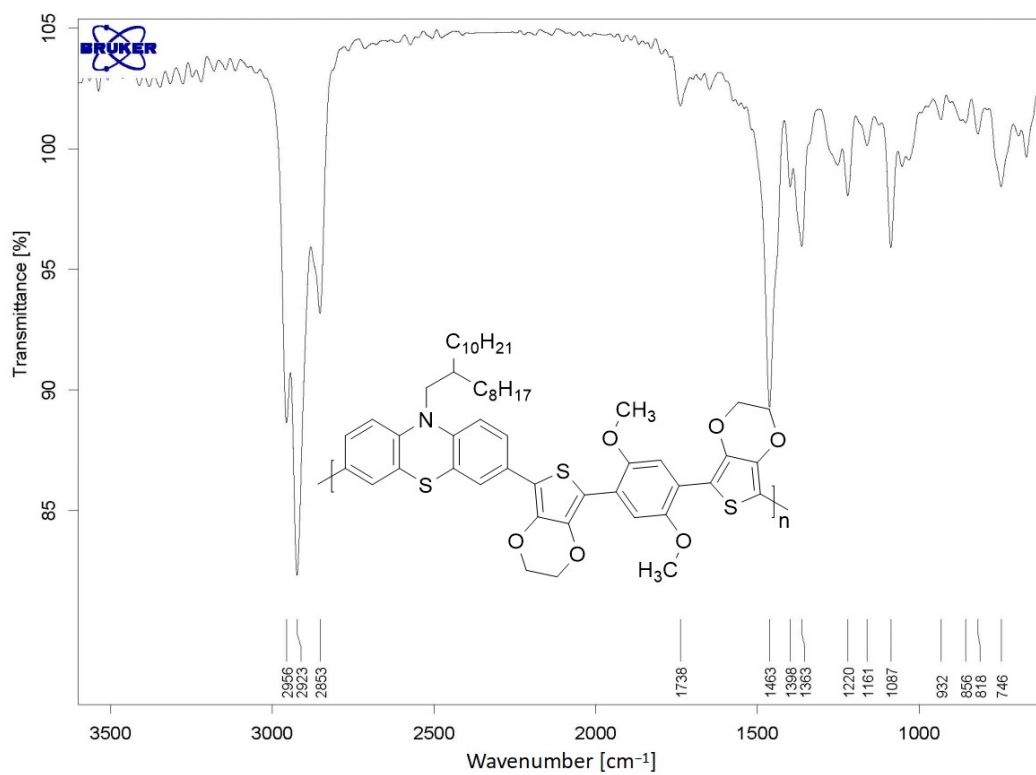
Fig. S18 ^{13}C NMR (100 MHz) spectrum of p-PTZ-EBEM in THF-d_8.

Fig. S19 ATR-FTIR spectrum of p-PTZ-EBEM.